AGU ADVANCING EARTH AND SPACE SCIENCE

Water Resources Research

RESEARCH ARTICLE
10.1029/2020WR028599

Tree Rings and Observations Suggest No Stable Cycles in Sierra Nevada Cool-Season Precipitation

A. P. Williams[1], K. J. Anchukaitis[1,2,3], C. A. Woodhouse[2,3], D. M. Meko[3], B. I. Cook[1,4], K. Bolles[1], and E. R. Cook[1]

[1]Department of Biology and Paleo Environment, Lamont-Doherty Earth Observatory of Columbia University, Palisades, NY, USA, [2]School of Geography, Development, and Environment, University of Arizona, Tucson, AZ, USA, [3]Laboratory of Tree-Ring Research, University of Arizona, Tucson, AZ, USA, [4]NASA Goddard Institute of Space Studies, New York, NY, USA

Key Points:

- Forty percent of 1902–2020 cool-season precipitation variability in California's Sierra Nevada range is accounted for by 2.2- and 13–15-year cycles
- Our novel tree-ring reconstruction captures these cycles and indicates that they have not been stable features over the past six centuries
- Extended periods of reconstructed cyclicity nonetheless suggest potentially untapped potential for statistical seasonal forecasting

Supporting Information:

- Supporting Information S1

Correspondence to:
A. P. Williams
williams@ldeo.columbia.edu

Citation:
Williams, A. P., Anchukaitis, K. J., Woodhouse, C. A., Meko, D. M., Cook, B. I., Bolles, K., & Cook, E. R. (2021). Tree rings and observations suggest no stable cycles in Sierra Nevada cool-season precipitation. *Water Resources Research*, *57*, e2020WR028599. https://doi.org/10.1029/2020WR028599

Received 14 AUG 2020
Accepted 28 NOV 2020

Abstract California's water resources rely heavily on cool-season (November–March) precipitation in the Sierra Nevada. Interannual variability is highly volatile and seasonal forecasting has little to no skill, making water management particularly challenging. Over 1902–2020, Sierra Nevada cool-season precipitation totals exhibited significant 2.2- and 13–15-year cycles, accounting for approximately 40% of total variability and perhaps signifying potential as seasonal forecasting tools. However, the underlying climate dynamics are not well understood and it is unclear whether these cycles are stable over the long term. We use tree rings to reconstruct Sierra Nevada cool-season precipitation back to 1400. The reconstruction is skillful, accounting for 55%–74% of observed variability and capturing the 20th-century 2.2- and 13–15-year cycles. Prior to 1900, the reconstruction indicates no other century-long periods of significant spectral power in the 2.2- or 13–15-year bands. The reconstruction does indicate significant cyclicity over other extended periods of several decades or longer, however, with dominant periodicities in the ranges of 2.1–2.7 and 3.5–8 years. The late 1700s through 1800s exhibited the highest-amplitude cycles in the reconstruction, with periodicities of 2.4 and 5.7–7.4 years. The reconstruction should serve to caution against extrapolating the observed 2.2- and 13–15-year cycles to guide future expectations. On the other hand, observations and the reconstruction suggest that interannual variability of Sierra Nevada cool-season precipitation is not a purely white noise process and research should aim to diagnose the dynamical drivers of extended periods of cyclicity in this critical natural resource.

1. Introduction

In California there is often too much or too little water. This was exemplified recently by the need for water-use restrictions during the severe drought from 2012 to 2016, followed immediately by a water surplus in water-year 2016–2017 that nearly caused northern California's Oroville Dam to overflow (Wang et al., 2017). Despite over a century of record keeping and management strategies that address this variability, the volatility of precipitation in California continues to pose major challenges to water resource managers. Management must minimize effects of drought on water supplies while also keeping reservoir levels low enough to minimize flood risk (Dettinger et al., 2011; Hanak et al., 2017; Stewart et al., 2020). California's exposure to hydrological volatility is particularly high because of its geographic setting: the majority of the state's surface water supply falls in the Sierra Nevada during the relatively short cool season of November–March (Dettinger, 2013; Dettinger et al., 2011, 2018), giving this region and season particular importance to California's water resources. While parts of the state, especially southern California, have worked to diversify water portfolios with a combination of surface, imported, and ground water, and to employ conservation measures and water markets (Gottlieb & FitzSimmons, 1991; Lund et al., 2018), California remains vulnerable to extreme variability of precipitation (Swain et al., 2018). Extreme hydrological shortages in the Sierra Nevada can be only moderately buffered by water supplies in regions and seasons not experiencing drought. California's drought and flood risk is amplified by the limited reliability of seasonal forecasts of Sierra Nevada precipitation (Jones et al., 2015). While forecast skill beyond a 2-week horizon is inherently poor globally, seasonal forecasting for parts of the western United States is aided by a teleconnection to the El Niño-Southern Oscillation (ENSO) (Huang et al., 2019; Seager & Hoerling, 2014). This is not the case, however, for the Sierra Nevada, which span the neutral point of the ENSO dipole that often drives

opposing precipitation anomalies in the Pacific Northwest versus the Southwest and supports most of the regional forecast skill (Dettinger et al., 1998; Wise, 2010; Cook et al., 2018).

The absence of reliable seasonal climate forecasts highlights the potential importance of the past as a guide to possible future variations in hydroclimate. Over the past century, the interannual variability of cool-season precipitation in the western United States, including the Sierra Nevada, exhibited some cyclic properties that could potentially aid prediction. These include a relatively strong periodicity at approximately 2.2 years (Dettinger et al., 1998; Granger, 1977; Johnstone, 2011) and a quasi-decadal periodicity at approximately 13–15 years (Ault & St. George, 2010; Dettinger et al., 1998; Florsheim & Dettinger, 2007; Johnstone, 2011). These quasi-cyclic features of precipitation appear unrelated to ENSO or the Pacific Decadal Oscillation (Ault & St. George, 2010). The observed tendency for cyclicity in western United States cool-season precipitation is intriguing because of the potential for statistical forecasting at seasonal to decadal scales. The 13–15-year periodicity has received particular attention from California's Department of Water Resources as a potential forecasting guide for decadal fluctuations in water supply (Meko et al., 2014, 2017; Wang et al., 2014). However, it is inadvisable to base forecasts on extrapolated observed cyclicity because the cyclicity may not be stable in time, particularly if the underlying dynamics are not well understood (Landsberg et al., 1963). Indeed, the dynamics driving the observed 2.2 and quasi-decadal precipitation cycles are unknown and both cycles appeared stronger in the second half of the 20th century than in the first half (Ault & St. George, 2010; Johnstone, 2011).

Tree-ring records present a unique opportunity to interrogate the stability of observed cyclicity in hydroclimate from a multicentury perspective. The western United States is particularly well-suited for such a test due to the high density of tree-ring records that are strongly correlated with cool-season precipitation (Fritts, 1965; Meko et al., 1993; St. George & Ault, 2014; Stahle et al., 2013, 2020; Williams et al., 2010). Tree-ring records in the western United States have been used extensively to reconstruct soil moisture and agricultural drought severity (Stockton & Meko, 1975; Cook et al., 1999, 2004; Williams et al., 2020), precipitation (Graumlich, 1993; Griffin & Anchukaitis, 2014; Diaz & Wahl, 2015; Wahl et al., 2017), streamflow (Meko et al., 2001, 2007; Woodhouse et al., 2020), and mountain snowpack (Belmecheri et al., 2016; Lepley et al., 2020; Pederson et al., 2011). However, these records have not been used extensively to extend our perspective on cyclicity in western United States cool-season precipitation. A notable exception is St. George and Ault (2014), who used tree-ring chronologies to investigate the history of observed 10–20-year periodicity in winter precipitation in the central latitudes of the United States west coast, observing that the amplitude of these cycles was highly inconsistent over the past 350 years. Tree-ring records have also been applied to examine cycles in California streamflow: A tree-ring study of the Sacramento and San Joaquin Rivers concluded that cyclic variation, with an average periodicity of about 15 years, is evident in both observations and reconstructions over the past 100 years, but is not a long-term feature of the hydroclimate of the basins (Meko et al., 2014). In addition, Wahl et al. (2020) used precipitation reconstructions to evaluate so-called flip-years in which a dry year is followed by a wet year or vice versa, which may be related to the observed 2.2-year periodicity of interest here, but cyclicity was not evaluated explicitly in that study.

The outsized importance of cool-season Sierra Nevada precipitation to California's water resources, the high interannual precipitation volatility, the apparent cyclicity, the limited capacity for seasonal forecasting, and the high density of precipitation-sensitive tree-ring chronologies in this region collectively motivate an investigation specifically focusing on the multicentennial history of cyclicity of cool-season precipitation the Sierra Nevada. A longer-term understanding of precipitation cyclicity in this region may guide expectations of whether it can be leveraged for forecasting and enhance our understanding of the climate dynamics that control cool-season precipitation variability at biennial to decadal timescales. Here we assess the observed spectral properties of Sierra Nevada cool-season precipitation and place them in the regional context across the western United States. We then produce a new 600-year tree-ring reconstruction of Sierra Nevada cool-season precipitation. We use this reconstruction to investigate the extent to which tree-ring reconstructions of hydroclimate faithfully capture the nuanced spectral properties of the observed 20th-century record and how Sierra Nevada cool-season precipitation cycles have varied over the past six centuries.

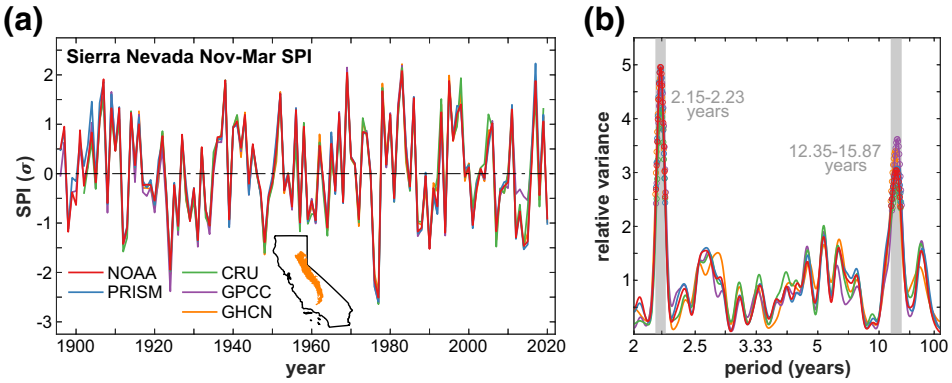

Figure 1. Sierra Nevada cool-season precipitation from five data sets. (a) November–March (Nov-Mar) Standardized Precipitation Index (SPI). Map inset: Sierra Nevada region in orange. (b) Spectra of the five time series in (a). Circles in (b) indicate significant (90%) difference from white noise.

2. Methods

2.1. Climate Data

The primary variable of interest is cool-season (November–March) precipitation, which we convert to the 5-month Standardized Precipitation Index (SPI) (McKee et al., 1993). The cool-season 5-month SPI expresses a time series of November–March precipitation totals in units of standard deviations (σ) from the mean after the time series has been transformed to have a normal distribution. The Sierra Nevada regional SPI record is the area-weighted mean of all gridded SPI time series in the Sierra Nevada region, which we then restandardize to have a mean of 0 and a standard deviation of 1 during 1921–2016 (the common period among the precipitation products considered). The boundary of the Sierra Nevada region, shown in Figure 1, is defined by the Environmental Protection Agency's level-3 ecoregions for California.

The primary observed precipitation dataset used in the United States is the National Oceanic and Atmospheric Administration (NOAA) 1/24° monthly Climgrid product, covering 1895–2020 (Vose et al., 2014). Alternate datasets used for comparison are the 1/24° PRISM dataset from Oregon State for 1895–2020 (Daly et al., 2008), the 1/2° version TS 4.04 Climate Research Unit (CRU) dataset for 1901–2019 (Harris et al., 2014), the 1/4° Global Precipitation Climatology Center (GPCC) v2018 dataset for 1901–2016 (Schneider et al., 2014), and a 1° dataset covering 1915–2020 that we calculate from raw daily precipitation totals at weather stations from the Global Historical Climate Network (GHCN). For that dataset, we use quantile mapping to gap-fill missing daily totals using records from nearby stations. We ultimately calculate cool-season SPI from 1352 gap-filled station records within the domain 28–53°N, 100–127°W. Each 1° gridded SPI record in our GHCN product is the restandardized mean of all station records within 0.75° of the grid's center.

For our reconstruction of gridded cool-season SPI and other analyses that extend beyond the United States, we compile a multiproduct dataset that uses NOAA Climgrid data in the United States and CRU in Canada and Mexico. Because the CRU dataset ends in 2019, we extend through 2020 using the 1/10° monthly ERA5-Land reanalysis from the European Center for Medium-Range Weather Forecasts, which covers 1981–2020 (Hersbach et al., 2020). We combine these datasets into a single 1/4° monthly precipitation dataset for 1901–2020 following Williams et al. (2020). For an analysis of the spectral properties of other elements of the water balance besides precipitation, we use 1/4° monthly reference evapotranspiration and 0–200 cm soil moisture plus snow water equivalent, updated from Williams et al. (2020). For our evaluation of how western North American precipitation relates to global climate, we use the 2° monthly mean NOAA Extended Sea Surface Temperature (SST) version 5 dataset for 1854–2020 and 2.5° monthly mean 500 hPa geopotential heights and zonally averaged equatorial wind velocity at 30 hPa from the reanalysis produced by the National Centers for Environmental Protection (NCEP) and Atmospheric Research (NCAR) for 1948–2020.

2.2. Cool-Season Precipitation Reconstruction

We produce a gridded reconstruction of cool-season SPI on a 1/2° grid within the region of 28–52°N, 105–128°W that covers years 1400–2000 of the Common Era. We then produce a Sierra Nevada reconstruction as the area-weighted average of gridded reconstructions within the Sierra Nevada region. A start year of 1400 is chosen because the availability of precipitation-sensitive tree-ring chronologies in the vicinity of the Sierra Nevada declines dramatically prior to that year. The observational dataset used as the reconstruction target was the 1/4° multiproduct 1901–2020 SPI dataset described above (based on NOAA Climgrid in the United States and CRU TS 4.04 beyond), but aggregated to 1/2° to reduce biases associated with reconstructing a high-resolution target field with more sparsely distributed tree-ring records.

For the gridded reconstruction, we consider a large network of 1364 standardized chronologies of western North American tree-Ring-Width Index (RWI) values with continuous coverage over at least 1800–2000. A RWI chronology is a standardized record of annual tree-ring widths that represents the average of generally at least 10, and often many more, trees at a site. The number of trees represented by a RWI chronology generally reduces further back in time as old trees are rarer than young trees. We deleted years from the beginning of a chronology if they were represented by less than three tree-ring specimens (which may have come from less than three trees). Growth trends unrelated to climate (e.g., negative trend in ring widths as trunk area increases) were removed using conservative detrending methods designed to preserve multicentennial growth variability likely due to climate (Melvin & Briffa, 2008). When applied to long ring-width time series of multiple centuries as was the case here, this method preserves high- to medium-frequency variance up to centennial or beyond, which is particularly important for our investigation of cyclicity on interannual to multidecadal scales. Section S7 of the Materials and Methods Supplemental text in Williams et al. (2020) provides additional information on this standardization approach. The RWI chronologies were calculated from raw measurements of tree-ring widths and these datasets were mostly obtained from the International Tree-Ring Databank (ITRDB). The network of RWI chronologies considered as potential predictors here is essentially the same as considered by Williams et al. (2020), which is an update and extension of the network used for prior gridded drought reconstructions (Cook et al., 2010b; Stahle et al., 2016, 2020). While many of the RWI records used in our study are known to be strong proxies for growing-season soil moisture, interannual variability in warm-season soil moisture across much of the study region, and the Sierra Nevada in particular, is dominated by cool-season precipitation (St. George & Ault, 2014; St. George et al., 2010). Many RWI records from the western United States are therefore ideal proxies for cool-season precipitation (Stahle et al., 2020). The network of RWI records also contains some chronologies collected specifically for their positive response to temperature. The ITRDB does not provide metadata on the intent of each collection, but our reconstruction method should only make use of these chronologies to the extent to which they reflect cool-season precipitation. RWI variability entrained into the reconstruction that is not associated with cool-season precipitation should contribute to reconstruction uncertainty.

Our reconstruction methods build from the point-by-point method developed for previous gridded hydroclimate reconstructions (Cook et al., 1999, 2004, 2010a, 2010b, 2015; Palmer et al., 2015; Stahle et al., 2016, 2020; Williams et al., 2020). For each grid cell, RWI chronologies are identified as candidate reconstruction predictors if they are located within a given search radius from the grid cell's center and correlate with the target time series during the calibration period (1902–2000) with at least 90% confidence based on a variety of correlation tests. To reduce redundancy among the predictor time series for a given reconstruction, a Principal Component Analysis (PCA) is performed on the RWI chronologies based on their covariance during 1800–2000. Principal Component Time Series (PCs) are then calculated as the sum of the RWI time series weighted by the PCA loading coefficients, covering the full period of overlap among all RWI time series. Only PCs with eigenvalues greater than the mean are retained as potential reconstruction predictors. The potential for these PCs as reconstruction predictors is assessed as the Pearson's correlation between each PC and the target SPI time series during 1902–2000 (r(PC,SPI)). A reconstruction model is developed in stepwise fashion by first using the PC with the highest absolute r(PC,SPI) as the primary predictor and then adding one PC at a time to a multiple regression in descending order of r(PC,SPI) for as long as the additional PC improves the model. Model improvement is assessed based on the Akaike Information Criterion with a bias correction for small sample size (AICc), a commonly used measure of model quality that includes a penalty for additional predictor variables (Akaike, 1974; Hurvich & Tsai, 1989), and the additional

PC must reduce the AICc by at least two for inclusion in the model and to continue the model-building process (Jones, 1985).

Often the length of the PCs, and therefore the reconstruction, does not extend back to 1400 because most RWI chronologies begin after that year. In that case, an additional reconstruction nest is developed by repeating the procedure above after discarding the RWI with the latest initial year. Additional years of reconstruction values from this secondary nest are appended to the beginning of the primary reconstruction. This is repeated until the primary reconstruction extends back to 1400.

Because RWI chronologies tend to have more temporal persistence than climate (Anderegg et al., 2015; Meko, 1981; Meko & Graybill, 1995), all RWI chronologies and observed cool-season SPI time series are prewhitened prior to the reconstruction procedure by removing autocorrelation using a low-order autoregressive model (Box et al., 2015), as is typical in tree-ring reconstruction of climate (Cook et al., 1999). After reconstruction of the prewhitened target time series, the autoregressive properties of the observed time series are added back to the reconstruction.

Reconstruction skill is assessed using an 11-fold leave-9-years-out cross validation. For each grid cell, the reconstruction procedure is repeated 11 times, each time withholding 9 consecutive years from the model calibration. Each of the 11 resultant reconstruction models is used to make out-of-sample reconstruction estimates for the 9 withheld years. Once out-of-sample estimates are made for the original 99-year calibration period (1902–2000), these estimates are appended and reconstruction skill is assessed as the coefficient of determination (R^2) between the out-of-sample time series and the target time series for 1902–2000 (referred to as the cross-validated R^2, or VR^2). We also assess the calibration R^2 (CR^2), which is the 1902–2000 R^2 between the final reconstruction (calibrated over the full calibration period) and the target SPI time series. For each grid cell, the VR^2 and CR^2 are calculated for each reconstruction nest to assess how reconstruction skill changes with declining availability of RWI chronologies. Reconstruction uncertainty intervals are produced using 10,000 Monte Carlo simulations of random time series of reconstruction errors that have the same mean, standard deviation, and autoregressive properties as the errors from the out-of-sample reconstruction estimates.

Our initial reconstruction considered RWI chronologies within a relatively small 75-km search radius from the center of each grid cell as potential predictors. However, the availability of RWI chronologies varies spatially and some areas do not have enough long, precipitation-sensitive RWI chronologies to allow for this relatively small 75-km search radius. In other areas with many nearby precipitation-sensitive chronologies, an even smaller search radius may be appropriate. Further, if RWI chronologies are widely distributed across a large search radius, it may be inappropriate for the target dataset to have a high 1/2° spatial resolution (Williams et al., 2020). For example, a 75-km search radius approximately overlaps a 1.5 × 1.5° box. We follow the Williams et al. (2020) ensemble-reconstruction approach in which an ensemble of alternate reconstructions are made considering varying search radii and spatial smoothings of the target dataset. We consider 18 alternative reconstructions with search radii ranging from 25 to 250 km and spatial smoothings ranging from no smoothing (original 1/2° resolution) to a 5 × 5-cell smoothing (2.5° resolution). For the no smoothing case, 3 × 3-cell smoothing case, and 5 × 5-cell smoothing case, the search radii vary from 25 to 175 km, 75 to 250 km, and 125 to 250 km, respectively. After producing the initial reconstruction with a 75-km search radius and 3 × 3-cell smoothing, each grid cell is offered the 18 alternative reconstructions for potential replacement in a stepwise manner that begins with the smallest search radius and least spatial smoothing. For each grid cell, the alternative reconstruction becomes the new primary reconstruction if the alternative reconstruction is ≥10 years longer than the primary reconstruction without reducing the VR^2 or increasing the cross-validated AICc or reduces the cross-validated AICc by at least two without reducing the VR^2 or reconstruction length. Notably, the maximum 250-km search radius considered here is smaller than the ≥450-km radius typically considered in gridded drought reconstructions (e.g., Cook et al., 1999; Stahle et al., 2020) in order to better capture fine-scale spatial variability in precipitation anomalies and minimize the influence of anomalies from surrounding areas on the Sierra Nevada precipitation reconstruction. This is important because regions to both the south and north have stronger ENSO teleconnections than are observed for the Sierra Nevada itself. After calculation of the area-weighted average reconstruction for the Sierra Nevada, we follow the bias correction method of Williams et al. (2020) to ensure that, for each unique set of RWI chronologies used in the reconstruction, the reconstructed time series has the same mean and variance as the observed regionally averaged SPI record during 1902–2000.

While Stahle et al. (2020) also produced seasonal precipitation reconstructions, we do not use those here because they used much larger search radii (500 and 1000 km), a shorter calibration period of 1928–1978, and a different definition of the cool season (December–April). The Stahle et al. reconstruction also did not include the out-of-sample reconstruction estimates made for each reconstruction nest. Our new reconstruction is meant to specifically optimize representation of Sierra Nevada precipitation, the period of overlap with observations to assess the reconstruction's ability to capture observed spectral properties, and the depth of information available regarding reconstruction skill.

Finally, our consideration of all available RWI chronologies as potential predictors could unduly contaminate our cool-season SPI reconstruction with extra climate information from chronologies sensitive to other seasons or variables. We therefore produce an alternative reconstruction with a prescreened set of RWI chronologies that correlate significantly ($p < 0.05$; Pearson's) with the nearest 1/2° grid cell's cool-season SPI record and correlate more strongly with cool-season SPI than with warm-season SPI, where two definitions of warm season are considered: April–October of the growth year and April–August of the growth year plus the preceding September–October. This screening reduces the original network to 396 chronologies. We also consider a second alternative reconstruction based on only 33 RWI chronologies from blue oaks, as that California-endemic species has exceptional ring-width sensitivity to cool-season precipitation (Griffin & Anchukaitis, 2014; Meko et al., 2011; Stahle et al., 2013).

2.3. Time Series Analysis

To assess the Sierra Nevada within the regional context of large-scale precipitation variability, we perform a PCA on the 1/4° multiproduct cool-season SPI dataset in the geographic domain of the North American west coast. We define the west coast as land area within 26–53°N, 105–129°W, and 750 km of the west coast. We use Pearson's correlation to assess the relationships between the leading PCs of west-coast cool-season SPI, Sierra Nevada cool-season SPI, and global geopotential heights and SSTs.

To evaluate cyclicity in the observed and reconstructed time series of cool-season Sierra Nevada SPI, we estimate spectra using the Blackman-Tukey smoothed-periodogram (Bloomfield, 2000; Chatfield, 1975). Wavelet analysis is used to investigate how spectral features of these time series evolved over the reconstruction period (Grinsted et al., 2004; Torrence & Compo, 1998). To extract time series of cycles associated with the dominant periodicities in an SPI time series, we use the single-channel Singular-Spectrum Analysis (SSA), which decomposes a single time series into PCs with discrete dominant periodicities (Allen & Smith, 1996; Vautard & Ghil, 1989; Vautard et al., 1992). To identify common dominant periodicities across many gridded SPI time series across the western United States, we use the Multitaper Singular Value Decomposition Method (MTM-SVD) (Ghil et al., 2002; Mann & Park, 1994, 1999).

3. Results and Discussion

Figure 1a shows records of Sierra Nevada cool-season SPI calculated from NOAA Climgrid and the four alternative data products for comparison. These datasets agree well ($R^2 > 0.93$) during the period of overlap. An exception is that the GPCC dataset does not indicate strong negative precipitation anomalies during 2012–2015, a period well known for extreme drought (Swain, 2015; Williams et al., 2015). We interpret that GPCC Sierra Nevada precipitation totals are erroneously high in 2012–2015, supported by disagreement between the GPCC record and that calculated from raw station records from the GHCN (orange line in Figure 1a).

Figure 1b shows the spectra for the five Sierra Nevada SPI time series shown in Figure 1a. All five records agree on significant spectral peaks centered on approximately 2.2 and 13–15 years. In the primary SPI record (NOAA), peak spectral activity is at periodicities of 2.18 and 13.9 years. Based on a Monte Carlo simulation with 10,000 random white-noise time series, the probability of either cycle arising randomly with its respective amplitude and periodicity is extremely low ($p = 0.0002$ and $p = 0.007$, respectively). However, a random time series can generate a high-amplitude cycle at any periodicity. Among the 10,000 random time series, just 1.25% contain a higher-amplitude cycle than that observed at the 2.18-year periodicity but nearly half (47.1%) had a higher-amplitude cycle than that observed at the 13.9-year periodicity. Consistent with the findings of Johnstone (2011), the SPI spectral peak near 2.2 years represents a distinctly shorter

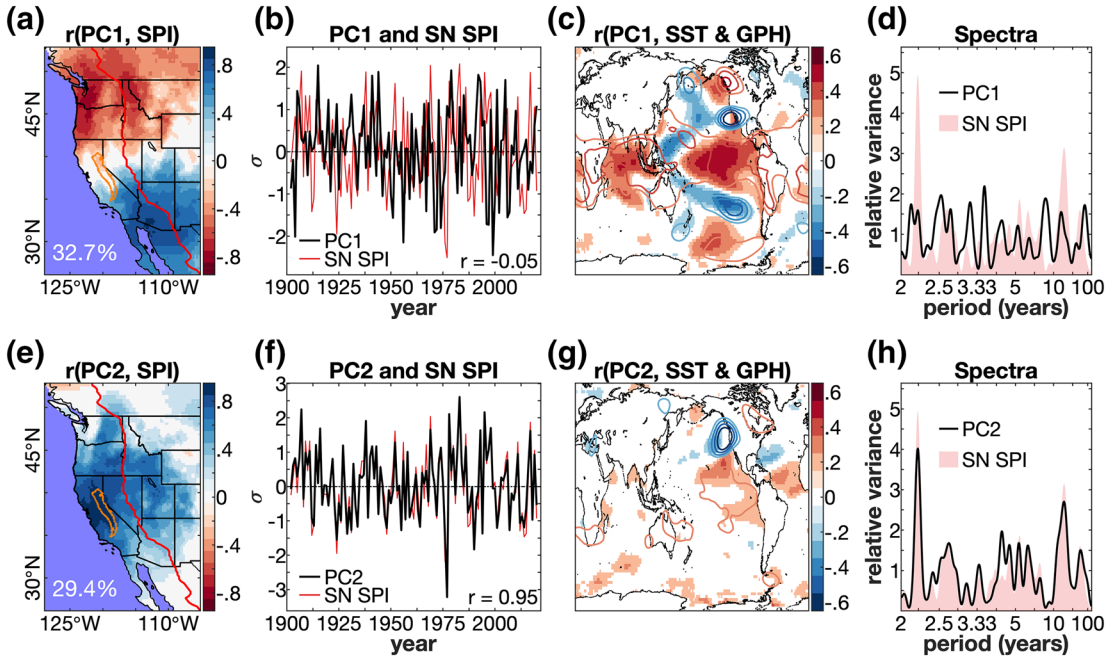

Figure 2. Dominant modes of cool-season (November–March) precipitation variability on the North American west coast. Top and bottom row panels represent the first (PC1) and second (PC2) modes of the Standardized Precipitation Index (SPI) in the North American west-coast region west of the red line in maps (a) and (e) based on a principal components analysis for water years 1902–2020. (a) Correlation between SPI and the PC1 time series (orange polygon: Sierra Nevada region; percentage values: variance of North American west-coast SPI contained in PC1). (b) PC1 time series (black) overlaid on Sierra Nevada SPI (SN SPI; red) (*r* value: correlation between PC1 and SN SPI; PC1 standardized to a 1921–2016 baseline). (c) Correlation between PC1 and cool-season mean Sea Surface Temperature (SST; background) and 500 hPa Geopotential Height (GPH; contours). Correlations in (c) were carried out on detrended time series over 1902–2020 and 1949–2020 for SST and GPH, respectively, and correlations corresponding to $p > 0.1$ are not shown. (d) Spectra of PC1 (black) and SN SPI (pink shading). (e)–(h) Same as (a)–(d) but for PC2.

periodicity than that of the Quasi-Biennial Oscillation (QBO); mean equatorial cool-season 30 hPa zonal wind velocity had a periodicity of 2.35 years during 1949–2020 (Figure S1).

The interannual variability and spectral properties of Sierra Nevada cool-season SPI are representative of cool-season precipitation across much of the midlatitude United States west coast (Figure 2). Based on the PCA, Sierra Nevada SPI is distinct from the well-known dipole mode associated with ENSO variability (PC1; Figures 2a–2d) and is instead consistent with a more spatially ubiquitous mode (PC2) described in previous work (Dettinger et al., 1998; Stewart et al., 2005; Wise, 2010; Cook et al., 2018; Baek et al., In press). Figure 2g shows that PC2 (and therefore Sierra Nevada cool-season precipitation) is associated with low geopotential heights off the United States west coast, but the lack of strong correlation with SSTs highlights the difficulty in seasonal forecasting based on ocean teleconnections.

Applying the MTM-SVD to cool-season SPI across the entire western United States (33–48°N, 105–125°W), we find that the dominant spectral peaks shared across the region are once again centered on periodicities of approximately 2.2 and 13–15 years (Figure S2). Figure 3 shows the contribution of these cycles to cool-season SPI across the western United States and in the Sierra Nevada specifically. The 2.2- and 13–15-year cycles have similar geographic footprints, with arcs of maximum influence extending north from central California through Oregon and Washington and east through northern Nevada, southern Idaho, northern Utah, and western Colorado (Figure 3 maps).

Performing an SSA on the observed Sierra Nevada SPI record, the two leading components have periodicities of 2.19 and 13.7 years, each accounting for 21–24% of the total variance of the 1902–2020 SPI time series (Figures 3a and 3b) and combining to account for approximately 40% of the total variance (Figure 3c time series). However, the contributions of 2.2- and 13–15-year cycles are not consistent throughout the observed period. These two SSA-derived components account for 46% of the observed Sierra Nevada SPI variability in 1941–2020, but only 24% in 1902–1940. This can be seen in the reduced amplitude of the 2.2- and 13–15-year

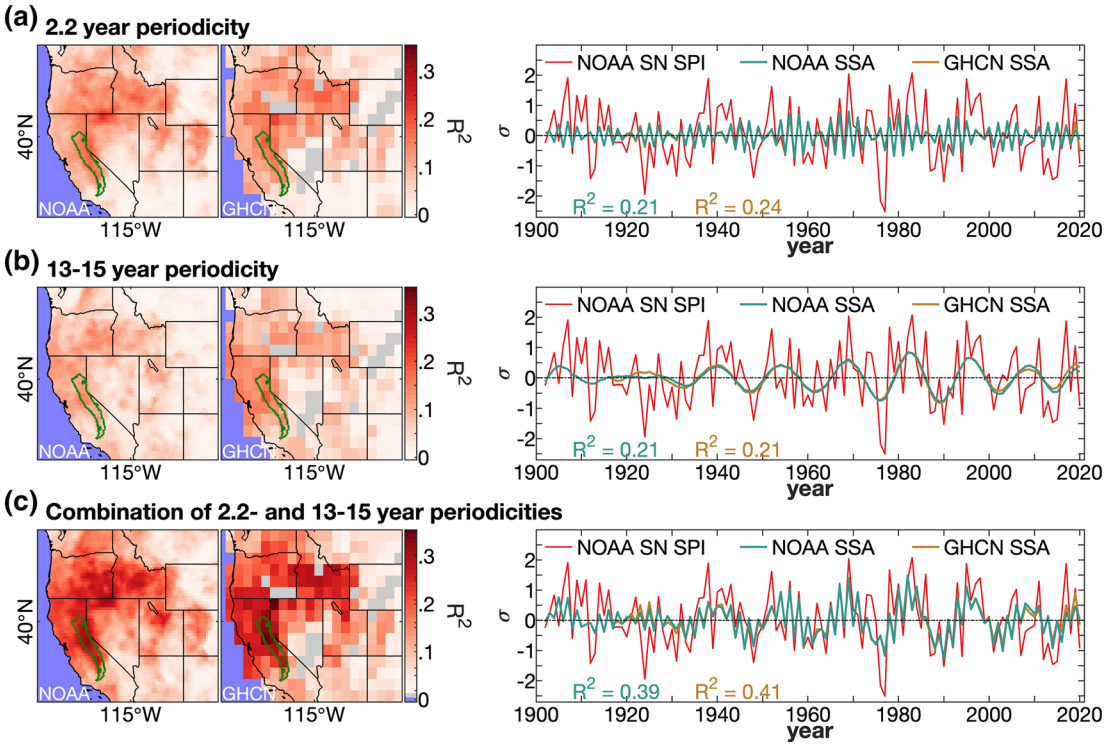

Figure 3. Dominant periodicities in western United States cool-season (November–March) Standardized Precipitation Index (SPI) based on the Multitaper Singular Value Decomposition Method (MTM-SVD) applied across the domain shown in the maps. (a) Maps: R^2 between the MTM-SVD-derived 2.2-year time series component and the original cool-season SPI record for (left) the NOAA Climgrid dataset during 1902–2020 and (right) the gridded GHCN dataset for 1916–2020 (gray: inadequate station coverage). Time series plot: (right) Sierra Nevada cool-season SPI calculated from NOAA Climgrid (NOAA SN SPI) overlaid by the 2.2-year time series component calculated by applying Singular-Spectrum Analysis (SSA) to (turquoise) NOAA Climgrid and (gold) GHCN. R^2 values indicate the fraction of Sierra Nevada cool-season SPI variance contained in the SSA-derived time series. (b) Same as (a) but for the 13–15-year component. (c) Same as (a) and (b) but for the sum of the 2.2- and 13–15-year components.

cycles in the time series plots of Figure 3, particularly between approximately 1910 and 1940. This reduction in decadal-scale variability is consistent with prior findings from the broader western United States (Ault & St. George, 2010; Johnstone, 2011). We observe the same result when we repeat the analyses with our GHCN-based SPI product (Figures 3 and S2).

What is the longer-term history of these observed spectral peaks in Sierra Nevada cool-season precipitation? Did the tendency for 2.2- and 13–15-year periodicities come and go with multidecadal persistence in prior centuries as they did during the observed period? Were other periodicities more dominant in prior centuries? We can address these questions if tree-ring reconstructions are skillful and can faithfully capture the spectral characteristics of cool-season precipitation variability during the 20th-century period of overlap with observations.

Figure 4 suggests that tree-ring reconstructions do a reasonable job at capturing the spectral properties of cool-season precipitation in the Sierra Nevada. Our gridded reconstructions are particularly skillful in California (Figure 4a), owing largely to the exceptional precipitation sensitivity of blue oak and big-cone Douglas-fir, both endemic to California (Meko et al., 2011; Michaelsen et al., 1987; Stahle et al., 2013). For the Sierra Nevada, our out-of-sample reconstruction estimates of regional mean SPI correlate highly ($VR^2 = 0.74$) with observations during the 1902–2000 period of overlap (Figure 4b). In addition to this remarkably high overall reconstruction skill, the Sierra Nevada reconstruction also captures multiple elements of the observed SPI spectra, including spectral peaks at periodicities of approximately 2.2 and 13–15 years (Figure 4c). While these spectral peaks are not as strong in the reconstruction as in the observations, the reconstruction's SSA-derived time series of the 2.2- and 13–15-year components still agree well with the observed 2.2- and 13–15-year time series components ($VR^2 = 0.57$), especially in the second half of the 20th century when observed variance at these periodicities was relatively high (Figure 4d). Notably,

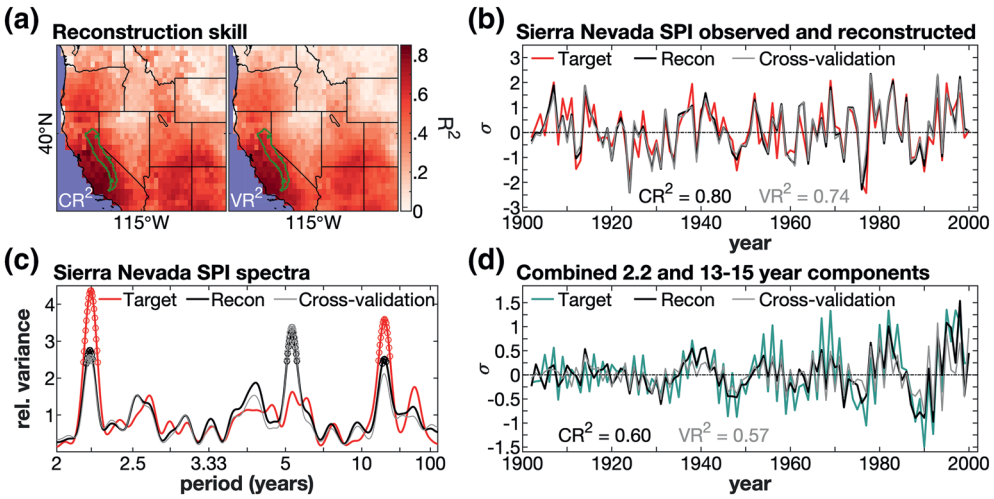

Figure 4. Comparison of reconstructed to observed cool-season (November–March) Standardized Precipitation Index (SPI). (a) R^2 between gridded SPI observations and reconstructions during the 1902–2000 period of overlap (left: fully Calibrated R^2 (CR^2) for the reconstruction calibrated on the full 1902–2000 period; right: cross-Validated R^2 (VR^2) of out-of-sample reconstruction estimates; gray grid cells: no reconstruction due to poor skill or lack of nearby tree-ring data). (b) Regionally averaged observed and reconstructed Sierra Nevada cool-season SPI during the period of overlap. (c) Spectra of the time series in (b). (d) Sum of the 2.2- and 13–15-year time series components of the SPI time series in (b) based on singular-spectrum analysis. In (b)–(d), black: primary reconstruction, gray: cross-validated reconstruction estimates. Reconstruction data are from the primary reconstruction based on all available tree-ring records covering 1800–2000. In (c), circles indicate significant (90%) difference from white noise.

the 2.2- and 13–15-year spectral peaks persist in alternate reconstructions in which the reconstruction is not forced to take on observed autoregressive properties and the 2.2- and 13–15-year cycles are subtracted away from observations using SSA. These results indicate that these reconstructed periodicities are due to actual periodicities in the tree-ring widths and not due to treatment of autoregressive properties in our reconstruction procedure.

One cause of the reconstruction's weaker spectral power at periodicities of 2.2 and 13–15 years is that the variance of the reconstruction during 1902–2000 is diluted by an additional 5.2-year cycle not present in the instrumental observations (Figure 4c). This reconstructed spectral peak corresponds to a 5.2-year cycle in soil moisture (Figure S3), which in turn corresponds to a spectral peak in warm-season precipitation that is likely enhanced by temporal autocorrelation of soil-moisture anomalies. This periodicity appears to arise as the average of multiple spectral peaks from various parts of the year as opposed to a single portion of the warm season (Figures S3c and S3d). Warm-season contamination of the cool-season SPI reconstruction highlights an inherent limitation of using tree-ring records, which integrate climatic variability over multiple seasons and years, to reconstruct one variable during one season. Because the reconstruction does not capture the full amplitudes of the observed 2.2- and 13–15-year cycles in cool-season precipitation, the reconstruction is prone to missing cyclicity entirely during periods when the real-world cyclicity has a low amplitude. For example, when the observed cool-season precipitation cyclicity was suppressed prior to approximately 1940, the reconstructed cyclicity is nearly absent (Figure 4d).

Our additional experiments with more restricted tree-ring networks show that these limitations of the reconstruction are not due to our use of all available tree-ring chronologies as potential predictors in our reconstruction. The 5.2-year periodicity and the reduced spectral power in the 2.2- and 13–15-year bands are also apparent in our two alternate reconstructions based only on RWI chronologies most representative of cool-season precipitation and on the blue oak chronologies (Figure S4).

Importantly, Figure 4 only represents the reconstruction nest that uses all available tree-ring chronologies that cover CE 1800–2000. For the reconstruction to extend further back in time, we must consider additional reconstruction nests developed from fewer tree-ring chronologies. This reduction in chronology availability leads to a general reduction in reconstruction skill of the Sierra Nevada SPI reconstruction, but

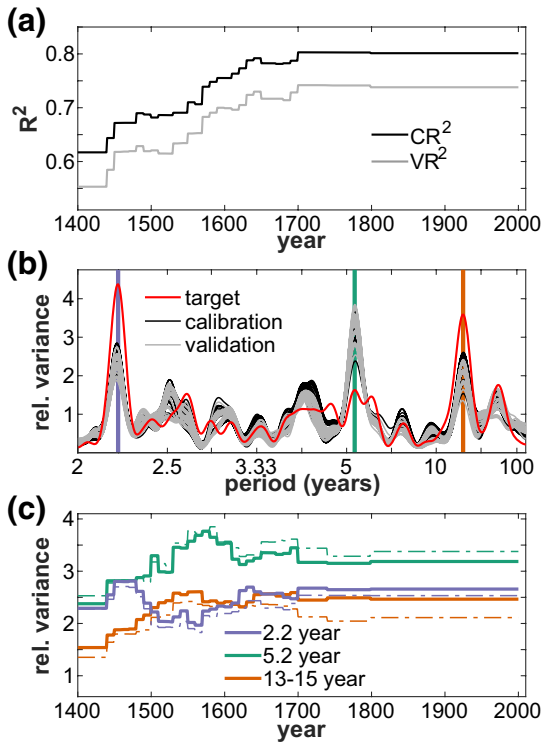

Figure 5. Reconstruction skill and spectra of the reconstruction nests used to reconstruct regionally averaged cool-season Sierra Nevada Standardized Precipitation Index (SPI) back to 1400. (a) R^2 between the reconstruction and observations during the 1902–2000 period of overlap. CR^2: R^2 based on the reconstruction calibrated to the full 1902–2000 period. VR^2: cross-validated R^2 based on out-of-sample reconstruction estimates. Each segment represents CR^2 and VR^2 values for a reconstruction nest based on a unique set of tree-ring chronologies. (b) Spectra of observed (red) and reconstructed Sierra Nevada cool-season SPI during 1902–2000. Each pair of black and gray spectra represent a unique reconstruction nest. Black: calibrated on the full 1902–2000 period. Gray: out-of-sample reconstruction estimates. (c) Time series of each reconstruction nest's relative variance values that correspond to spectral peaks at periodicities of 2.2, 5.2, and 13–15 years from (b).

it remains high ($VR^2 \geq 0.55$) back to 1400 (Figure 5a). All reconstruction nests agree on the general 1902–2000 spectral characteristics evident in the primary reconstruction nest, but there are nonetheless fluctuations in how well reconstructions capture the observed spectral peaks at 2.2 and 13–15 years as well as the spectral peak at 5.2 years (Figure 5b). As the number of available tree-ring chronologies declines further back in time, there is no discernable trend in the ability of the reconstruction to capture the variance attributed to the 2.2-year periodicity. However, the nests used to reconstruct SPI prior to 1530 exhibit a markedly reduced ability to capture the amplitude of the observed 13–15-year cycle (Figure 5c). The reduced ability of very long reconstructions to capture the amplitude of the observed 13–15-year cycles, and the degraded reconstruction skill in general among these long reconstructions, are largely due to the absence of northern California blue oak chronologies prior to 1530.

Based on our results, we suggest caution in interpreting reconstructed spectral characteristics of Sierra Nevada cool-season precipitation. While the reconstruction should capture real-world spectral peaks when there is a high degree of amplitude at these periodicities, Figures 4 and 5 suggest that the reconstruction's ability to do so is likely to change as the network of available tree-ring chronologies changes and that the amplitude of reconstructed cyclicity is muted relative to the real world. Reconstructed spectra are also confounded by other climate and soil-moisture conditions besides cool-season precipitation.

Figure 6a shows the full reconstruction of Sierra Nevada cool-season SPI. While the purpose of the current study is to inspect spectral properties, we briefly point out that similar to previous findings from this region (Diaz & Wahl, 2015; Graumlich, 1993; Griffin & Anchukaitis, 2014; Wahl et al., 2017; Woodhouse et al., 2020), the recent period of instrumental observations does not appear to capture the full range of Sierra Nevada cool-season precipitation anomalies. In particular, the reconstruction indicates a single-year negative SPI value in 1580 (−4.18 σ) that greatly exceeds the severity of the most negative SPI in the observed record (1977: −2.43 σ). Remarkably, 1580 and 1977 were each the second year in a pair of back-to-back extreme drought years (1579–1580 and 1976–1977), with 1579 ranking second most negative in the reconstruction (−2.31 σ) and 1976 ranking second most negative in the observations (−2.04 σ). In an analysis of the distribution of running-mean SPI values, in which a range of window lengths was considered, the observed SPI record does not fully represent the potential for exceptionally dry multiyear periods, but overrepresents the potential for wet multiyear periods (Figure S5).

Our analysis also suggests that the spectral properties of cool-season precipitation during the observed period were not representative of those of prior centuries. The spectral analysis in Figure 6b shows that the 600-year reconstruction as a whole does not have a significant spectral peak at the 2.2-year periodicity over its complete length, but does contain several prominent spectral peaks at periodicities of 2.4–2.6, 4.6–7.5, 12.8, and 21.3 years (Figure 6b). The wavelet analysis in Figure 6c indicates that none of these spectral peaks were stable features throughout the reconstruction. While this may be due to the limitation of the reconstruction discussed above, we know from instrumental observations that the early 1900s also exhibited far less spectral activity at the 2.2- and 13–15-year periodicities than in more recent decades. The reconstruction suggests that this early 1900s period was part of a rare period from approximately 1875 to 1950 when there was little coherent cyclicity at any periodicity (Figure 6c). Notably, this period of reduced spectral power coincides with a prolonged absence of single-year wet-to-dry or dry-to-wet transitions in the California precipitation reconstruction evaluated by Wahl et al. (2020). The most consistent spectral feature of the reconstruction is a broad tendency for periodicities of 3.5–8.0 years (Figure 6c). However, we advise

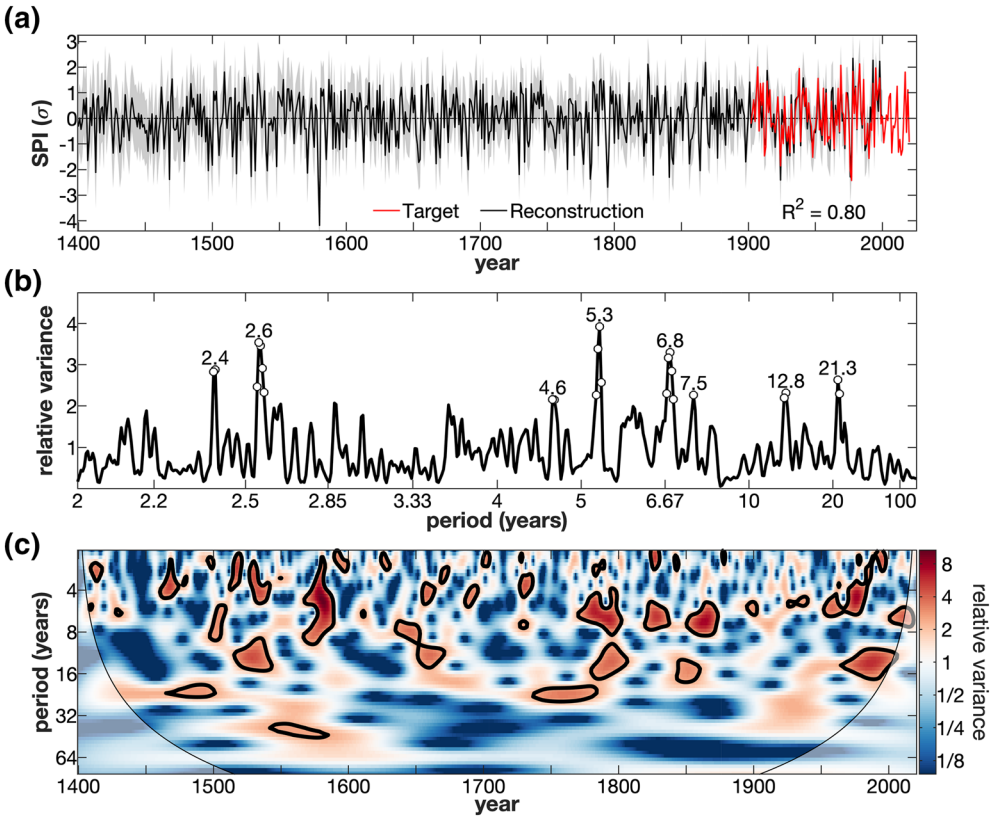

Figure 6. Reconstructed cool-season (November–March) Sierra Nevada Standardized Precipitation Index (SPI) and spectral features. (a) Time series of (black) the reconstruction for 1400–2000 and (red) the target observational SPI record for 1902–2020. Gray: 95% confidence intervals. R^2: coefficient of determination between fully calibrated reconstruction and observations during 1902–2020. (b) Spectra of the reconstruction. Numbers above spectral peaks: period (years) associated with each peak. (c) Wavelet of reconstruction. Circles in (b) and bold black lines in (c) significant (90%) difference from white noise. In (b) and (c), the reconstruction was extended with observations for 2001–2020.

against confident interpretation of this as a true spectral feature of cool-season precipitation given that this spectral band contains the reconstructed artificial 5.2-year cycle during the observed period. These results are consistent with those obtained from our alternate reconstruction based on the prescreened network of tree-ring chronologies that are particularly sensitive to cool-season precipitation (Figure S6).

For more direct assessment of the 20th-century spectral features in a 600-year context, Figure 7 evaluates the reconstruction's spectral properties on a centennial scale. In Figure 7a, the spectra for each of the six centuries of the reconstruction share few commonalities, further supporting the conclusion that the strong 2.2- and 13–15-year cycles in Sierra Nevada cool-season precipitation during the 20th century were unique and cannot be reliably used for forecasting. Once again, all results shown in Figure 7 are consistent with those obtained from the alternate reconstruction based on the prescreened network of tree-ring chronologies (Figure S7).

Figure 7b presents the same centennial spectral analysis as in Figure 7a, but as a Hovmöller diagram in which the spectral analysis is performed on the reconstruction along a 99-year moving window. Here it is further clarified that the 20th century was unique in terms of all three of its significant spectral peaks. Prior to 1857–1955, no reconstructed 99-year period exhibits significance in any of the 2.2-, 5.2-, or 13–15-year bands. However, Figure 7 highlights some interesting general tendencies throughout the reconstruction. While the 20th century was unique in terms of the 2.2-year cycle, spectral peaks coinciding broadly with 2.1-year and/or 2.4–2.7-year periodicities are more consistent throughout the reconstruction. Particularly strong spectral peaks indicate a high degree of variance associated with a 2.4-year cycle from the late 1700s

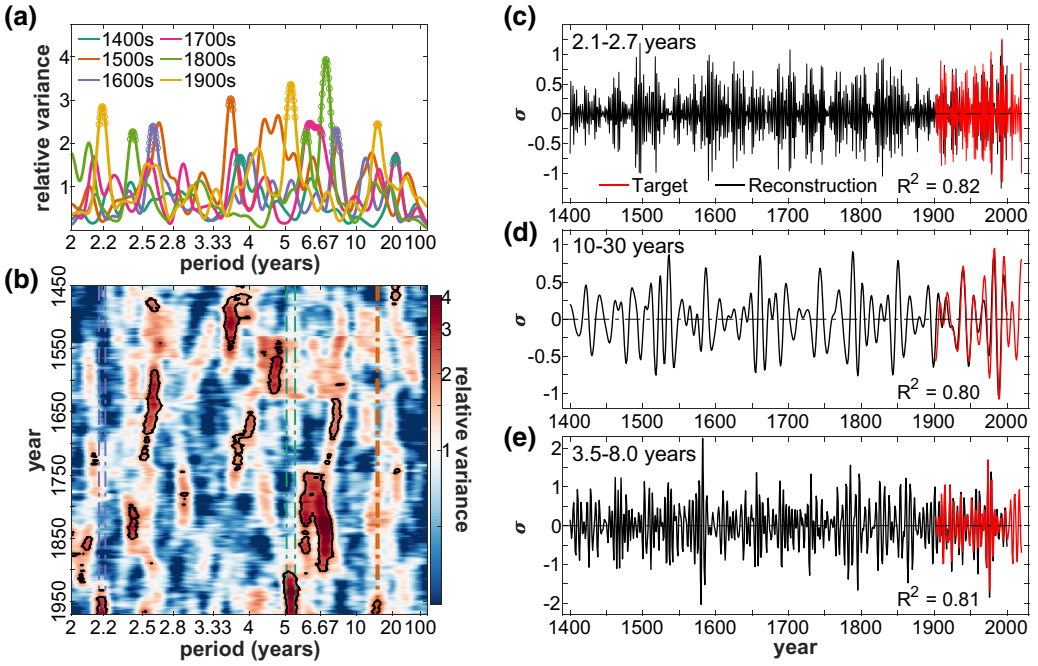

Figure 7. Assessment of stability of Sierra Nevada cool-season Standardized Precipitation Index (SPI) spectra over the past 600 years (a) Spectra during each of the six centuries of the SPI reconstruction. (b) Ninety-nine-year moving-window spectral analysis (*y* axis: center year of each 99-year period). In (b), observed SPI values for 2001–2020 are appended to the reconstruction. The three pairs of vertical dotted lines in (b) bound the significant 2.2-, 5.2-, and 13–15-year periodicities indicated in the 1900s in (a). Circles in (a) and black contours in (b) indicate significant (90%) difference from white noise. (c)–(e) Band-pass filtered time series of the (black) reconstruction and (red) observations in the (c) high, (d) low, and (e) midfrequency spectral bands indicated in the top-left of each panel. R^2 in (c)–(e): coefficient of determination between the fully-calibrated reconstruction and observations during 1902–2020.

through mid-1800s and a 2.6-year cycle from the late 1500s to early 1700s. Similarly, while spectral power in the 13–15-year band is only evident in the observed period, there is a broad tendency for decadal variability in the 10–30-year timeframe throughout the reconstruction. It is not clear whether these tendencies for quasi-biennial and quasi-decadal variations were driven by consistent climatological mechanisms throughout the reconstruction, nor the degree to which the reconstructed drift in periodicities within each spectral band may have been promoted by noise in the climate and/or ecological system. Regardless, the band-pass filtered time series shown in Figures 7c and 7d indicate that the amounts of variance concentrated in these broad 2.1–2.7- and 10–30-year spectral bands are highly inconsistent throughout the reconstruction. This suggests that even if the large-scale climatological mechanisms driving quasi-biennial and quasi-decadal periodicity have remained the same over the past six centuries, their amplitudes and/or the amplitudes of the Sierra Nevada precipitation responses to these mechanisms have been irregular.

Finally, Figures 7b and 7e allow us to inspect the high degree of reconstructed 3.5–8-year spectral activity in more detail. While each century exhibited significant spectral power somewhere in this broad subdecadal band, there was little consistency in the peak periodicity from century to century. The peak reconstructed spectral activity in this or any spectral band was from the late 1700s to late 1800s and corresponded to periodicities of approximately 5.7–7.4 years. The mid-1700s through late 1800s also coincided with the highest degree of variance attributed to a 2.4-year periodicity in the reconstruction. Prior to that, the reconstruction indicates higher-frequency (3.5–5-year) variability. Given that the reconstructed 5.2-year cycle during the 20th century was unrelated to cool-season precipitation, extra caution is necessary when deciding whether these reconstructed periods of high-amplitude activity in the 3.5–8-year window reflect true cool-season precipitation cyclicity. Further, the cooler temperatures of the Little Ice Age, particularly the 1700s (Graumlich, 1993), may have promoted even more artificial midfrequency variability by enhancing the persistence of soil-moisture anomalies. On the other hand, lack of midfrequency variability in observed cool-season precipitation is no guarantee that reconstructions of preobservational mid-frequency variability

are artificial. For example, Wise (2010) and DeRose et al. (2013) show that the latitude of the middle-point of the western United States ENSO precipitation dipole appears to have varied over past centuries. An unstable ENSO teleconnection may be expected to promote temporal variability in the spectral characteristics of Sierra Nevada cool-season precipitation, particularly in the 3.5–8 year band. The prominence of midfrequency variability throughout the reconstruction, and its lack of prominence in observations, should be the focus of further research.

4. Conclusions

Instrumental observations indicate significant cool-season precipitation cycles with periodicities of 2.2 and 13–15 years in the Sierra Nevada and much of midlatitude western North America, which do not appear to be directly related to tropical SST teleconnections. These observed cycles were particularly strong from approximately 1940 to present. However, these cycles had substantially lower amplitudes in the early 1900s, suggesting that the strengths and periodicities of precipitation cycles may not be stable in time. Our goal was to determine whether tree-ring reconstructions can capture the observed cyclicity in Sierra Nevada cool-season precipitation, and if so, how cyclicity has varied over the past several centuries.

Our tree-ring reconstruction of Sierra Nevada cool-season precipitation is highly skillful and captures the observed 2.2- and 13–15-year cycles, though with somewhat muted amplitudes. The reconstruction also contains a 20th-century spectral peak at 5.2 years that was not observed, but instead resulted from hydrological conditions integrated throughout the year. The network of tree-ring chronologies used for the Sierra Nevada reconstruction changes back in time due to declining availability of chronologies, and this reduces skill, particularly prior to 1530s when blue oak chronologies in northern California are unavailable. This shift toward less precipitation-sensitive tree-ring records prior to the mid-1500s does not cause the reconstruction to lose its ability to capture high-frequency 2.2-year spectral power, but does reduce the reconstruction's reliability to capture spectral power in the 13–15-year window. These results serve as caution against over-confidence in the reconstruction's ability to capture the full spectral properties of cool-season precipitation. For example, even if a spectral feature such as a 2.2-year cycle was strong and stable over 1400–2000 in real-world precipitation, our results suggest the tree-ring reconstruction would underrepresent the cycle's amplitude and stability.

Despite limitations inherent to our reconstruction's ability to capture nuanced spectral features of seasonal precipitation, the near-absence of significant reconstructed 2.2- and 13–15-year cycles prior to the observed period strongly suggests that these were not stable features of cool-season precipitation over the past 600 years. This is consistent with previous tree-ring based findings that 10–20-year cyclicity in midlatitude west-coast winter precipitation was uniquely strong in the 20th century (St. George & Ault, 2011) and that a near-15-year cycle in 20th-century Sacramento and San Joaquin river flow was a transient phenomenon (Meko et al., 2014). Interestingly, our reconstruction indicates much more consistent spectral activity in the 2.4–2.6-year band and other tendencies toward 2.1- and 10–30-year cycles. The highest-amplitude spectral activity in the reconstruction is in the 4.6–7.5-year timeframe, but this should be interpreted with skepticism due to the reconstruction's artificial 5.2-year spectral peak in the 20th century. The strongest reconstructed cyclicity in the entire reconstruction occurs in the 4.6–7.5-year band during the Little Ice Age period.

Although the observed 2.2- and 13–15-year cycles were most likely not stable over the past several centuries, observations and our reconstruction indicate that precipitation cycles can emerge and persist for several decades at a time. Our results caution against extrapolating observed cycles into the future for water-management purposes, but the tendency for multidecade persistence of periodicity remains intriguing. More work is needed to understand the dynamical drivers of multidecade periods of phase-locked periodicity, which may aid future management decisions regarding whether an ongoing cycle is likely persist into the future. But it also must be kept in mind that anthropogenic forcing increasingly reduces the applicability of historical conditions as guides for future expectations. Future work should investigate the degree to which general circulation models simulate multidecadal persistence of interannual to decadal cycles such as those observed and reconstructed here, and use model experiments to diagnose the drivers of cyclicity. Results may expose teleconnections and/or external forcing mechanisms that promote Sierra Nevada precipitation cyclicity, or may reveal that multidecadal persistence of Sierra Nevada precipitation cycles such as those

observed and reconstructed should be expected to come and go from random atmospheric variability alone. Models may also be useful to guide expectations as to whether transient cycles in cool-season precipitation should be enhanced (in amplitude and/or persistence) or suppressed by anthropogenic climate forcing and/or phases of natural decadal variability such as the Pacific Decadal Oscillation. Anthropogenic climate change incentivizes continued work to understand the drivers of Sierra Nevada cool-season precipitation cyclicity, as water management in California is likely to become increasingly difficult due to increasing evaporative demand, reduced capacity for mountain snowpack to regulate runoff, and increased precipitation volatility (Barnett et al., 2005, 2008 ; Berg & Hall, 2015; Gershunov et al., 2019; Pendergrass et al., 2017; Pierce et al., 2018; Swain et al., 2018; Livneh & Badger, 2020; Williams et al., 2020)

Data Availability Statement

All climate data used are publicly available: NOAA Climgrid (http://dx.doi.org/10.7289/V5SX6B56), PRISM from Oregon State University (www.prism.oregonstate.edu), CRU 4.04 (https://crudata.uea.ac.uk/cru/data/hrg/cru_ts_4.04), GPCC (https://opendata.dwd.de/climate_environment/GPCC/html/fulldata-monthly_v2018_doi_download.html), GHCN (https://www.ncdc.noaa.gov/ghcnd-data-access), ERA5 (https://cds.climate.copernicus.eu/cdsapp#!/dataset/reanalysis-era5-land-monthly-means), NOAA Extended SSTs (https://psl.noaa.gov/data/gridded/data.noaa.ersst.v5.html), and NCEP/NCAR geopotential heights (https://psl.noaa.gov/data/gridded/data.ncep.reanalysis.html), monthly stratospheric zonal winds for QBO analysis (https://psl.noaa.gov/data/climateindices/list/), and Williams et al. (2020) reference evapotranspiration and soil moisture (https://dx.doi.org/10.25921/2vbe-8092). Publicly available tree-ring data come from the International Tree-Ring Databank (https://www.ncdc.noaa.gov/data-access/paleoclimatology-data). The EPA ecoregion map data used to define the Sierra Nevada region was accessed from https://www.epa.gov/eco-research/level-iii-and-iv-ecoregions-state. All observed and reconstructed precipitation grids and Sierra Nevada annual time series are available at https://www.ldeo.columbia.edu/~williams/wrr2020data/.

Acknowledgments
This work would not be possible without the tree-ring data from many gracious contributors, largely through the International Tree-Ring Databank hosted by the National Oceanic and Atmospheric Administration. Special thanks to Jeremy Littell, who collected, developed, and shared ring-width measurements for 18 RWI chronologies in Idaho, Oregon, and Washington. Funding came from NSF AGS-1703029 (A. P. Williams, K. Bolles, and E. R. Cook), NSF AGS-1803995 (K. J. Anchukaitis), NASA 16-MAP16-0081 (A. P. Williams and B. I. Cook); and NOAA MAPP NA19OAR4310278 (A. P. Williams and B. I. Cook). LDEO contribution #8476.

References

Akaike, H. (1974). A new look at the statistical model identification. *IEEE Transactions on Automatic Control*, *19*(6), 716–723. https://doi.org/10.1109/TAC.1974.1100705

Allen, M. R., & Smith, L. A. (1996). Monte Carlo SSA: Detecting irregular oscillations in the presence of colored noise. *Journal of Climate*, *9*(12), 3373–3404. https://doi.org/10.1175/1520-0442(1996)009<3373:MCSDIO>2.0.CO;2

Anderegg, W. R. L., Schwalm, C., Biondi, F., Camarero, J. J., Koch, G., Litvak, M., et al. (2015). Pervasive drought legacies in forest ecosystems and their implications for carbon cycle models. *Science*, *349*(6247), 528–532. https://doi.org/10.1126/science.aab1833

Ault, T. R., & St George, S. (2010). The magnitude of decadal and multidecadal variability in North American precipitation. *Journal of Climate*, *23*(4), 842–850. https://doi.org/10.1175/2009JCLI3013.1

Baek, S. H., Smerdon, J. E., Cook, B. I., & Williams, A. P. (In press). US Pacific coastal droughts are predominantly driven by internal atmospheric variability. *Journal of Climate*, –. http://dx.doi.org/10.1175/jcli-d-20-0365.1

Barnett, T. P., Adam, J. C., & Lettenmaier, D. P. (2005). Potential impacts of a warming climate on water availability in snow-dominated regions. *Nature*, *438*(7066), 303–309.

Barnett, T. P., Pierce, D. W., Hidalgo, H. G., Bonfils, C., Santer, B. D., Das, T., et al. (2008). Human-induced changes in the hydrology of the western United States. *Science*, *319*(5866), 1080–1083. https://doi.org/10.1126/science.1152538

Belmecheri, S., Babst, F., Wahl, E. R., Stahle, D. W., & Trouet, V. (2016). Multi-century evaluation of Sierra Nevada snowpack. *Nature Climate Change*, *6*(1), 2–3. https://doi.org/10.1038/nclimate2809

Berg, N., & Hall, A. (2015). Increased interannual precipitation extremes over California under climate change. *Journal of Climate*, *28*(16), 6324–6334. https://doi.org/10.1175/JCLI-D-14-00624.1

Bloomfield, P. (2000). *Fourier analysis of time series: An introduction* (2nd ed.). New York, NY: John Wiley & Sons.

Box, G. E. P., Jenkins, G. M., Reinsel, G. C., & Ljung, G. M. (2015). *Time series analysis: Forecasting and control* (5th ed.). Hoboken, NJ: John Wiley & Sons.

Chatfield, C. (1975). *The analysis of time series: Theory and practice*. Boston, MA: Springer. Retrieved from https://link.springer.com/book/10.1007/978-1-4899-2925-9#about

Cook, E. R., Anchukaitis, K. J., Buckley, B. M., D'Arrigo, R. D., Jacoby, G. C., & Wright, W. E. (2010a). Asian monsoon failure and megadrought during the last millennium. *Science*, *328*(5977), 486–489. https://doi.org/10.1126/science.1185188

Cook, E. R., Meko, D. M., Stahle, D. W., & Cleaveland, M. K. (1999). Drought reconstructions for the continental United States. *Journal of Climate*, *12*(4), 1145–1162. https://doi.org/10.1175/1520-0442(1999)012<1145:DRFTCU>2.0.CO;2

Cook, E. R., Seager, R., Heim, R. R., Jr, Vose, R. S., Herweijer, C., & Woodhouse, C. (2010b). Megadroughts in North America: Placing IPCC projections of hydroclimatic change in a long-term palaeoclimate context. *Journal of Quaternary Science*, *25*(1), 48–61. https://doi.org/10.1002/jqs.1303

Cook, E. R., Seager, R., Kushnir, Y., Briffa, K. R., Büntgen, U., Frank, D., et al. (2015). Old world droughts and pluvials during the Common Era. *Science Advances*, *1*(10), e1500561. https://doi.org/10.1126/sciadv.1500561

Cook, B. I., Williams, A. P., Seager, R., Smerdon, J. E., Singh, D., & Mankin, J. S. (2018). Revisiting the leading drivers of Pacific coastal drought variability in the Contiguous United States. *Journal of Climate*, *31*, 25–43. https://doi.org/10.1175/JCLI-D-17-0172.1

Cook, E. R., Woodhouse, C. A., Eakin, C. M., Meko, D. M., & Stahle, D. W. (2004). Long-term aridity changes in the western United States. *Science*, *306*(5698), 1015–1018. https://doi.org/10.1126/science.1102586

Daly, C., Halbleib, M., Smith, J. I., Gibson, W. P., Doggett, M. K., Taylor, G. H., et al. (2008). Physiographically sensitive mapping of climatological temperature and precipitation across the conterminous United States. *International Journal of Climatology*, *28*(15), 2031–2064. https://doi.org/10.1002/joc.1688

DeRose, R. J., Wang, S.-Y., & Shaw, J. D. (2013). Feasibility of high-density climate reconstruction based on Forest Inventory and Analysis (FIA) collected tree-ring data. *Journal of Hydrometeorology*, *14*(1), 375–381.

Dettinger, M. D. (2013). Atmospheric rivers as drought busters on the US West Coast. *Journal of Hydrometeorology*, *14*(6), 1721–1732. https://doi.org/10.1175/JHM-D-13-02.1

Dettinger, M. D., Alpert, H., Battles, J. J., Kusel, J., Safford, H., Fougeres, D., et al. (2018). *Sierra Nevada summary. Report California's fourth climate change assessment (No. SUM-CCCA4-2018-004).*. California Energy Commission/Natural Resources Agency. Retrieved from https://pubs.er.usgs.gov/publication/70201117

Dettinger, M. D., Cayan, D. R., Diaz, H. F., & Meko, D. M. (1998). North-south precipitation patterns in western North America on interannual-to-decadal timescales. *Journal of Climate*, *11*(12), 3095–3111. https://doi.org/10.1175/1520-0442(1998)011<3095:NSPPIW>2.0.CO;2

Dettinger, M. D., Ralph, F. M., Das, T., Neiman, P. J., & Cayan, D. R. (2011). Atmospheric rivers, floods and the water resources of California. *Water*, *3*(2), 445–478 https://doi.org/10.3390/w3020445

Diaz, H. F., & Wahl, E. R. (2015). Recent California water year precipitation deficits: A 440-year perspective. *Journal of Climate*, *28*(12), 4637–4652. https://doi.org/10.1175/JCLI-D-14-00774.1

Florsheim, J. L., & Dettinger, M. D. (2007). Climate and floods still govern California levee breaks. *Geophysical Research Letters*, *34*(22), L22403. https://doi.org/10.1029/2007GL031702

Fritts, H. C. (1965). Tree-ring evidence for climatic changes in western North America. *Monthly Weather Review*, *93*(7), 421–443. https://doi.org/10.1175/1520-0493(1965)093<0421:TREFCC>2.3.CO;2

Gershunov, A., Shulgina, T., Clemesha, R. E. S., Guirguis, K., Pierce, D. W., Dettinger, M. D., et al. (2019). Precipitation regime change in Western North America: The role of atmospheric rivers. *Scientific Reports*, *9*, 9944. https://doi.org/10.1038/s41598-019-46169-w

Ghil, M., Allen, M. R., Dettinger, M. D., Ide, K., Mann, M. E., Robertson, A. W., et al. (2002). Advanced spectral methods for climatic time series. *Reviews of Geophysics*, *40*(1), 3–1. https://doi.org/10.1029/2000RG000092

Gottlieb, R., & FitzSimmons, M. (1991). *Thirst for growth: Water agencies as hidden government in California.*. Tucson, AZ: University of Arizona Press.

Granger, O. E. (1977). Secular fluctuations of seasonal precipitation in lowland California. *Monthly Weather Review*, *105*(4), 386–397. https://doi.org/10.1175/1520-0493(1977)105<0386:SFOSPI>2.0.CO;2

Graumlich, L. J. (1993). A 1000-year record of temperature and precipitation in the Sierra Nevada. *Quaternary Research*, *39*(2), 249–255. https://doi.org/10.1006/qres.1993.1029

Griffin, D., & Anchukaitis, K. J. (2014). How unusual is the 2012–2014 California drought?. *Geophysical Research Letters*, *41*, 9017–9023. https://doi.org/10.1002/2014GL062433

Grinsted, A., Moore, J. C., & Jevrejeva, S. (2004). Application of the cross wavelet transform and wavelet coherence to geophysical time series. *Nonlinear Processes in Geophysics, European Geosciences Union*, *11*(5–6), 561–566.

Hanak, E., Chappelle, E., Escriva-Bou, A., Gray, B., Jezdimirovic, J., McCann, H., & Mount, J. (2017). *Priorities for California's water* (Vol. October). San Francisco, CA: Public Policy Institute of California. Retrieved from https://www.ppic.org/wp-content/uploads/r_1017ehr.pdf

Harris, I., Jones, P. D., Osborn, T. J., & Lister, D. H. (2014). Updated high-resolution grids of monthly climatic observations—The CRU TS3.10 Dataset. *International Journal of Climatology*, *34*(3), 623–642. https://doi.org/10.1002/joc.3711

Hersbach, H., Bell, B., Berrisford, P., Hirahara, S., Horányi, A., Muñoz-Sabater, J., et al. (2020). The ERA5 global reanalysis. *Quarterly Journal of the Royal Meteorological Society*, *146*(730), 1999–2049. https://doi.org/10.1002/qj.3803

Huang, B., Shin, C.-S., & Kumar, A. (2019). Predictive skill and predictable patterns of the US seasonal precipitation in CFSv2 reforecasts of 60 years (1958–2017). *Journal of Climate*, *32*(24), 8603–8637. https://doi.org/10.1175/JCLI-D-19-0230.1

Hurvich, C. M., & Tsai, C.-L. (1989). Regression and time series model selection in small samples. *Biometrika*, *76*(2), 297–307. https://doi.org/10.1093/biomet/76.2.297

Johnstone, J. A. (2011). A quasi-biennial signal in western US hydroclimate and its global teleconnections. *Climate Dynamics*, *36*(3–4), 663–680. https://doi.org/10.1007/s00382-010-0755-9

Jones, R. S. (1985). Time series analysis—Time domain. In A. H. Murphy, & R. W. Katz (Eds.), *Probability, statistics, and decision making in the atmospheric sciences* (pp. 223–259). Boulder, CO: Westview Press.

Jones, J., Anderson, M., Chung, F., Islam, N., Juricich, R., Kofoid, J., et al. (2015). *California's most significant droughts: Comparing historical and recent conditions* (Vol. February). Sacramento, CA: California Department of Water Resources. Retrieved from https://cawaterlibrary.net/wp-content/uploads/2017/05/CalSignficantDroughts_v10_int.pdf

Landsberg, H., Mitchell, J. Jr, Crutcher, H. L., & Quinlan, F. (1963). Surface signs of the biennial atmospheric pulse. *Monthly Weather Review*, *91*(10–12), 549–556. https://doi.org/10.1175/1520-0493(1963)091<0549:SSOTBA>2.3.CO;2

Lepley, K., Touchan, R., Meko, D., Shamir, E., Graham, R., & Falk, D. (2020). A multi-century Sierra Nevada snowpack reconstruction modeled using upper-elevation coniferous tree rings (California, USA). *The Holocene*. https://doi.org/10.1177/0959683620919972

Livneh, B., & Badger, A. M. (2020). Drought less predictable under declining future snowpack. *Nature Climate Change*, *10*, (5), 452–458. http://dx.doi.org/10.1038/s41558-020-0754-8

Lund, J., Medellin-Azuara, J., Durand, J., & Stone, K. (2018). Lessons from California's 2012–2016 drought. *Journal of Water Resources Planning and Management*, *144*(10), 04018067. https://doi.org/10.1061/(ASCE)WR.1943-5452.0000984

Mann, M. E., & Park, J. (1994). Global-scale modes of surface temperature variability on interannual to century timescales. *Journal of Geophysical Research*, *99*(D12), 25819–25833. https://doi.org/10.1029/94JD02396

Mann, M. E., & Park, J. (1999). Oscillatory spatiotemporal signal detection in climate studies: A multiple-taper spectral domain approach. *Advances in Geophysics*, *41*, 1–131. https://doi.org/10.1016/S0065-2687(08)60026-6

McKee, T. B., Doesken, N. J., & Kleist, J. (1993). The relationship of drought frequency and duration to time scales. In Proceedings of the 8th conference on applied climatology (Vol. 17, pp. 179–183). Boston, MA: American Meteorological Society. Retrieved from https://climate.colostate.edu/pdfs/relationshipofdroughtfrequency.pdf

Meko, D. M. (1981). *Applications of Box-Jenkins methods of time series analysis to the reconstruction of drought from tree rings (Dissertation)*. Tucson, AZ: Hydrology and Water Resources Graduate College, University of Arizona. Retrieved from https://repository.arizona.edu/handle/10150/191062

Meko, D. M., & Graybill, D. A. (1995). Tree-ring reconstruction of upper Gila River discharge. *Water Resources Bulletin*, *31*(4), 605–616. https://doi.org/10.1111/j.1752-1688.1995.tb03388.x

Meko, D. M., Stahle, D. W., Griffin, D., & Knight, T. A. (2011). Inferring precipitation-anomaly gradients from tree rings. *Quaternary International*, *235*(1), 89–100. https://doi.org/10.1016/j.quaint.2010.09.006

Meko, D. M., Stockton, C. W., Hughes, M. K., Cook, E. R., & Stahle, D. W. (1993). Spatial patterns of tree-growth anomalies in the United States and southeastern Canada. *Journal of Climate*, *6*(9), 17731786. https://doi.org/10.1175/1520-0442(1993)006<1773:SPOTGA>2.0.CO;2

Meko, D. M., Therrell, M. D., Baisan, C. H., & Hughes, M. K. (2001). Sacramento river flow reconstructed to AD 869 from tree rings. *JAWRA Journal of the American Water Resources Association*, *37*(4), 1029–1039. https://doi.org/10.1111/j.1752-1688.2001.tb05530.x

Meko, D. M., Woodhouse, C. A., Baisan, C. A., Knight, T., Lukas, J. J., Hughes, M. K., & Salzer, M. W. (2007). Medieval drought in the Upper Colorado River Basin. *Geophysical Research Letters*, *34*, L10705. https://doi.org/10.1029/2007GL029988

Meko, D. M., Woodhouse, C. A., & Bigio, E. R. (2017). *Southern California tree-ring study (final report for the California Department of Water Resources, No. 4600011071*, p. 123). Tucson, AZ: University of Arizona. Retrieved from https://pdfs.semanticscholar.org/fbaf/487604e2537c8f51037035e59c13113edeeb.pdf

Meko, D. M., Woodhouse, C. A., & Touchan, R. (2014). *Klamath/san joaquin/sacramento hydroclimatic reconstructions from tree rings (final report to California department of water resources, Agreement 4600008850*, p. 66). Sacramento, CA: California Department of Water Resources. Retrieved from https://cwoodhouse.faculty.arizona.edu/sites/cwoodhouse.faculty.arizona.edu/files/FinalCAWDReport.pdf

Melvin, T. M., & Briffa, K. R. (2008). A "signal-free" approach to dendroclimatic standardisation. *Dendrochronologia*, *26*(2), 71–86. https://doi.org/10.1016/j.dendro.2007.12.001

Michaelsen, J., Haston, L., & Davis, F. W. (1987). 400 years of central California precipitation variability reconstructed from tree-rings. *Journal of the American Water Resources Association*, *23*(5), 809–818. https://doi.org/10.1111/j.1752-1688.1987.tb02956.x

Palmer, J. G., Cook, E. R., Turney, C. S. M., Allen, K., Fenwick, P., Cook, B. I., et al. (2015). Drought variability in the eastern Australia and New Zealand summer drought atlas (ANZDA, CE 1500–2012) modulated by the Interdecadal Pacific Oscillation. *Environmental Research Letters*, *10*(12), 124002. https://doi.org/10.1088/1748-9326/10/12/124002

Pederson, G. T., Gray, S. T., Woodhouse, C. A., Betancourt, J. L., Fagre, D. B., Littell, J. S., et al. (2011). The unusual nature of recent snowpack declines in the North American Cordillera. *Science*, *333*(6040), 332–335. https://doi.org/10.1126/science.1201570

Pendergrass, A. G., Knutti, R., Lehner, F., Deser, C., & Sanderson, B. M. (2017). Precipitation variability increases in a warmer climate. *Scientific Reports*, *7*(1), 17966. https://doi.org/10.1038/s41598-017-17966-y

Pierce, D. W., Kalansky, J. F., & Cayan, D. R. (2018). *Climate, drought, and sea level rise scenarios* (California's Fourth Climate Change Assessment No. CNRA-CEC-2018-006). Sacramento, CA: California Energy Commission. Retrieved from https://www.energy.ca.gov/sites/default/files/2019-11/Projections_CCCA4-CEC-2018-006_ADA.pdf

Schneider, U., Becker, A., Finger, P., Meyer-Christoffer, A., Ziese, M., & Rudolf, B. (2014). GPCC's new land surface precipitation climatology based on quality-controlled in situ data and its role in quantifying the global water cycle. *Theoretical and Applied Climatology*, *115*(1–2), 15–40. https://doi.org/10.1007/s00704-013-0860-x

Seager, R., & Hoerling, M. (2014). Atmosphere and ocean origins of North American droughts. *Journal of Climate*, *27*, 4581–4606. https://doi.org/10.1175/JCLI-D-13-00329.1

Stahle, D. W., Cook, E. R., Burnette, D. J., Torbenson, M. C. A., Howard, I. M., Griffin, D., et al. (2020). Dynamics, variability, and change in seasonal precipitation reconstructions for North America. *Journal of Climate*, *33*(8), 3173–3195. https://doi.org/10.1175/JCLI-D-19-0270.1

Stahle, D. W., Cook, E. R., Burnette, D. J., Villanueva, J., Cerano, J., Burns, J. N., et al. (2016). The Mexican Drought Atlas: Tree-ring reconstructions of the soil moisture balance during the late pre-Hispanic, colonial, and modern eras. *Quaternary Science Reviews*, *149*, 34–60. https://doi.org/10.1016/j.quascirev.2016.06.018

Stahle, D. W., Griffin, R. D., Meko, D. M., Therrell, M. D., Edmondson, J. R., Cleaveland, M. K., et al. (2013). The ancient blue oak woodlands of California: Longevity and hydroclimatic history. *Earth Interactions*, *17*(12), 1–23. https://doi.org/10.1175/2013EI000518.1

Stewart, I. T., Cayan, D. R., & Dettinger, M. D. (2005). Changes toward earlier streamflow timing across western North America. *Journal of Climate*, *18*(8), 1136–1155. https://doi.org/10.1175/JCLI3321.1

Stewart, I. T., Rogers, J., & Graham, A. (2020). Water security under severe drought and climate change: Disparate impacts of the recent severe drought on environmental flows and water supplies in Central California. *Journal of Hydrology X*, *7*, 100054. https://doi.org/10.1016/j.hydroa.2020.100054

St George, S., Ault, A., & T. R. (2011). Is energetic decadal variability a stable feature of the central Pacific Coast's winter climate?. *Journal of Geophysical Research: Atmospheres*, *116*, D12102. https://doi.org/10.1029/2010JD015325

St George, S., & Ault, T. R. (2014). The imprint of climate within Northern Hemisphere trees. *Quaternary Science Reviews*, *89*, 1–4. https://doi.org/10.1016/j.quascirev.2014.04.029

St George, S., Meko, D. M., & Cook, E. R. (2010). The seasonality of precipitation signals embedded within the North American Drought Atlas. *The Holocene*, *20*(6), 983–988. https://doi.org/10.1177/0959683610365937

Stockton, C. W., & Meko, D. M. (1975). A long-term history of drought occurrence in western United States as inferred from tree rings. *Weatherwise*, *28*(6), 244–249. https://doi.org/10.1080/00431672.1975.9931775

Swain, D. L. (2015). A tale of two California droughts: Lessons amidst record warmth and dryness in a region of complex physical and human geography. *Geophysical Research Letters*, *42*, 9999–10003. https://doi.org/10.1002/2015GL066628

Swain, D. L., Langenbrunner, B., Neelin, J. D., & Hall, A. (2018). Increasing precipitation volatility in twenty-first-century California. *Nature Climate Change*, *8*, 427–433. https://doi.org/10.1038/s41558-018-0140-y

Torrence, C., & Compo, G. P. (1998). A practical guide to wavelet analysis. *Bulletin of the American Meteorological Society*, *79*(1), 61–78. https://doi.org/10.1175/1520-0477(1998)079<0061:APGTWA>2.0.CO;2

Vautard, R., & Ghil, M. (1989). Singular spectrum analysis in nonlinear dynamics, with applications to paleoclimatic time series. *Physica D: Nonlinear Phenomena*, *35*(3), 395–424. https://doi.org/10.1016/0167-2789(89)90077-8

Vautard, R., Yiou, P., & Ghil, M. (1992). Singular-spectrum analysis: A toolkit for short, noisy chaotic signals. *Physica D: Nonlinear Phenomena*, *58*(1–4), 95–126. https://doi.org/10.1016/0167-2789(92)90103-T

Vose, R. S., Applequist, S., Squires, M., Durre, I., Menne, M. J., Williams Jr, C. N., et al. (2014). Improved historical temperature and precipitation time series for US climate divisions. *Journal of Applied Meteorology and Climatology*, *53*(5), 1232–1251. https://doi.org/10.1175/JAMC-D-13-0248.1

Wahl, E. R., Diaz, H. F., Vose, R. S., & Gross, W. S. (2017). Multicentury evaluation of recovery from strong precipitation deficits in California. *Journal of Climate*, *30*(15), 6053–6063. https://doi.org/10.1175/JCLI-D-16-0423.1

Wahl, E. R., Hoell, A., Zorita, E., Gille, E., & Diaz, H. F. (2020). A 450-year Perspective on California Precipitation "Flips.". *Journal of Climate*, *33*(23), 10221–10237. https://doi.org/10.1175/JCLI-D-19-0828.1

Wang, J., Yin, H., Reyes, E., & Chung, F. (2014). Quasi-decadal oscillation in the CMIP5 and CMIP3 climate model simulations: California case. In Fall Meeting of the American Geophysical Union (Vol. 2014, H23N1077). San Francisco, CA: American Geophysical Union. Retrieved from https://ui.adsabs.harvard.edu/abs/2014AGUFM.H23N1077W/abstract

Wang, S.-Y. S., Yoon, J.-H., Becker, E., & Gillies, R. (2017). California from drought to deluge. *Nature Climate Change*, *7*(7), 465–468. https://doi.org/10.1038/nclimate3330

Williams, A. P., Cook, E. R., Smerdon, J. E., Cook, B. I., Abatzoglou, J. T., Bolles, K., et al. (2020). Large contribution from anthropogenic warming to a developing North American megadrought. *Science*, *368*(6488), 314–318. https://doi.org/10.1126/science.aaz9600

Williams, A. P., Michaelsen, J., Leavitt, S. W., & Still, C. J. (2010). Using tree-rings to predict the response of tree growth to climate change in the continental United States during the 21st century. *Earth Interactions*, *14*(19), 1–20. https://doi.org/10.1175/2010EI362.1

Williams, A. P., Seager, R., Abatzoglou, J. T., Cook, B. I., Smerdon, J. E., & Cook, E. R. (2015). Contribution of anthropogenic warming to California drought during 2012-2014. *Geophysical Research Letters*, *42*, 6819–6828. https://doi.org/10.1002/2015GL064924

Wise, E. K. (2010). Spatiotemporal variability of the precipitation dipole transition zone in the western United States. *Geophysical Research Letters*, *37*, L07706. https://doi.org/10.1029/2009GL042193

Woodhouse, C. A., Meko, D. M., & Bigio, E. R. (2020). A long view of southern California water supply: Perfect droughts revisited. *JAWRA Journal of the American Water Resources Association*, *56*(2), 212–229. https://doi.org/10.1111/1752-1688.12822